Available online at www.sciencedirect.com
SCIENCE DIRECT®
Journal of Power Sources 118 (2003) 256–264
JOURNAL OF POWER SOURCES
www.elsevier.com/locate/jpowsour

Synthesis of nanocrystalline materials for SOFC applications by acrylamide polymerisation

A. Tarancón*, G. Dezanneau, J. Arbiol, F. Peiró, J.R. Morante

Departament d'Electrónica, Universitat de Barcelona, Martí i Franquès 1, 08028 Barcelona, Spain

Abstract

Ultrafine powders with applicability in solid oxide fuel cells (SOFCs) were prepared by a novel method based on a polyacrylamide gel-combustion process: $Zr_{0.84}Y_{0.16}O_{1.92}$ (8YSZ), $Ce_{0.8}Gd_{0.2}O_{1.9}$ (CGO), $La_{0.9}Sr_{0.1}Ga_{0.8}Mg_{0.2}O_{2.85}$ (LSGM), $La_2Mo_2O_9$, $La_{0.8}Sr_{0.2}CoO_{3-\delta}$ (LSC) and $La_{0.8}Sr_{0.2}FeO_{3-\delta}$ (LSF). Synthesized powders present desirable characteristics for powder consolidation and sintering, including nanometric crystal size (10–40 nm), narrow size distribution and the possibility of aggregate disagglomeration via soft ball milling. A classical screen-printing method is presented as a novel thin dense layer deposition technique. First results on deposition of quasi-full-density thin films of 8YSZ (around 5 μm thick) were obtained at a sintering temperature of 1300 °C with sintering times of 10 h in air.

Keywords: SOFC; Synthesis; Acrylamide; Methacrylamide; Screen-printing; Dense electrolyte

1. Introduction

Solid ionic and mixed ionic-electronic conductors (MIECs) have received special attention in recent years in relation to their applicability in solid oxide fuel cells (SOFCs) [1,2] as electrolyte and electrode materials, respectively. Fluorite (i.e. $Zr_{0.84}Y_{0.16}O_{1.92}$ (8YSZ), $Ce_{0.8}Gd_{0.2}O_{1.9}$ (CGO)), perovskite (i.e. $La_{0.9}Sr_{0.1}Ga_{0.8}Mg_{0.2}O_{2.85}$ (LSGM)), BIMEVOX and the recently discovered LAMOX [3] (i.e. $La_2Mo_2O_9$) families fulfil special structural requirements for fast oxygen conduction. The mixed ionic-electronic conductivity and catalytic properties present in doped $LaMO_3$ (M = transition metals) perovskite materials transform compounds like $La_{0.8}Sr_{0.2}CoO_{3-\delta}$ (LSC) [4] and $La_{0.8}Sr_{0.2}FeO_{3-\delta}$ (LSF) [2] into good candidates for cathode use in fuel cells.

Dense electrolytes with a high area/thickness ratio which minimizes Ohmic loss in SOFCs can be obtained by thick film fabrication technologies such as tape casting and slip casting. Similarly, electrodes with a determined microstructure (graded composition, controlled porosity...) can be obtained by screen-printing technology. In both cases, electrolyte and electrodes processing requires submicron materials with a controlled morphology, which conventional solid state chemistry paths are unable to provide. Uncontrolled crystalline growth, composition inhomogeneities, grain size non-uniformity are other disadvantages of classical methods. Wet chemistry routes provide interesting alternatives because the mixing of species occurs on the atomic scale, cations being dissolved in solution. Co-precipitation, spray–freezing, sol–gel and Pechini [5] are the state-of-the-art methods.

The sol–gel process starts from molecular precursors (generally alkoxides) and forms a solid network by hydrolysis condensation reactions. Because of the different chemical behavior of each cation, it is difficult to control the reaction mechanisms for the synthesis of binary or ternary oxides. The Pechini method [5] is based on forming a solid polymer resin with cations chelated on it in homogeneous manner. Cations in solution with a hydroxycarboxylic acid (e.g. citric acid) as chelating agent mixed with a polyhydroxy alcohol (e.g. ethylene glycol) produce polyesterification at medium temperatures.

An improvement of the previous synthetic routes consists in the formation of an auxiliary three-dimensional (3D) tangled network, of polyacrylamide gel, in which a solution of the respective chelated cations is soaked [6–8]. A steric entrapment of stoichiometric cation solution occurs in nanocavities formed inside the gel, that is, an homogeneous microsolution with cations in the desired stoichiometry. This method is time-saving in relation to the Pechini method because the artificial gel formation at low temperature is rapid compared with the progressive transformation from viscous to resin in the Pechini method.

* Corresponding author.
E-mail address: tarancon@el.ub.es (A. Tarancón).

0378-7753/03/$ – see front matter © 2003 Elsevier Science B.V. All rights reserved.
doi:10.1016/S0378-7753(03)00091-0

This method based on wet chemistry is presented here as a means to synthesize ultrafine and highly homogeneous powders of $Zr_{0.84}Y_{0.16}O_{2-\delta}$ (8YSZ), $Ce_{0.8}Gd_{0.2}O_{1.9}$ (CGO), $La_{0.9}Sr_{0.1}Ga_{0.8}Mg_{0.2}O_{3-\delta}$(LSGM), $La_2Mo_2O_9$ for electrolyte and $La_{0.9}Sr_{0.1}CoO_{3-\delta}$ (LSC), $La_{0.9}Sr_{0.1}FeO_{3-\delta}$ (LSF) for cathode materials. One of the aims of this work was to point out the versatility and robustness of this method by preparing up to seven different compositions for SOFC applications without significant changes in the manufacturing process. Fluorite compounds are studied in detail in order to give a general example of the method, while attention will be addressed to specific points of the synthesis for the other compositions. The other aim of this work was to present first results of an alternative novel technique for manufacturing thin dense layers (<10 μm) based on a screen-printing method. Screen-printing has been typically used in SOFCs to deposit porous layers with high specific surface area to perform the electrode role. Starting with polyacrylamide-assisted synthesized powders of 8YSZ, a slurry with appropriate rheological properties was prepared and screen printed as a thin dense layer showing a real scalable alternative to traditional electrolyte manufacturing (sintered pellets, tape casting, slip casting, . . .). Other reports of the same method with $Sm_{0.2}Ce_{0.8}O_{1.9}$ [9] also show good results.

1.1. Experimental

1.1.1. Precursors and synthesis of final compounds

Individual aqueous solutions of metallic cations were prepared from nitrate salts. Nitrates used were $Y(NO_3)_3{\cdot}6H_2O$, $ZrO(NO_3)_2{\cdot}xH_2O$, $Ce(NO_3)_3{\cdot}6H_2O$, $Gd(NO_3)_3{\cdot}6H_2O$, $La(NO_3)_3{\cdot}6H_2O$, $Co(NO_3)_3{\cdot}6H_2O$, $Fe(NO_3)_3{\cdot}9H_2O$, $Ga(NO_3)_3{\cdot}xH_2O$, $Sr(NO_3)_2$, $Y(NO_3)_3{\cdot}6H_2O$ $La(NO_3)_3$. The formula mass ratio of $ZrO(NO_3)_2{\cdot}xH_2O$ (resp. $Ga(NO_3)_3{\cdot}xH_2O$) was determined by weighing the resulting ZrO_2 mass (resp. Ga_2O_3), obtained from the calcination of a known amount of precursor at 900 °C during 8 h. An aqueous solution (pH controlled via NH_4OH) of ethylenediaminetetraacetic acid (H_4EDTA) as a chelating agent was added in 1:1 ratio assuming the formation of a chelate with formula $[MeEDTA]^{\delta-4}$ ($Me^{+\delta}$ = metallic cation). Solutions of chelated cations were mixed in stoichiometric ratio in aqueous solution and homogenized by magnetic stirring. Finally, auxiliary 3D network components were dissolved: the monomers of acrylamide ($CH_2{=}CHCONH_2$) to form chains of polyacrylamide and the cross-linker *N*,*N*′-methylene-bis-acrylamide ($CH_2{=}CHCONHCH_2NHCOCH{=}CH_2$) to achieve final gel complex topology. The polymerisation was initiated by thermo-polymerisation when the solution reached 80 °C via addition of α,α′-azoisobutyronitrile (AIBN, $C_8H_{12}N_4$) initiator dissolved in a few ml of acetone. The gel was then dried for a few minutes in a microwave oven. The xerogels obtained were then homogenized in a ceramic mortar and submitted to one subsequent thermal treatment. The thermal treatment applied was a heating ramp of 300 °C/h up to the holding temperature (800 °C) during 5 h, followed by a free cooling, the whole process under air. For the LSGM series of samples, subsequent thermal treatments were performed in order to study the evolution of parasitic phases with temperature. Alternatively to acrylamide (high toxicity), methacrylamide (moderate risk) was used as a monomer in the $La_2Mo_2O_9$ and LSC syntheses without changes in the procedure followed.

1.1.2. Powder structural characterization

XRD powder patterns were collected at room temperature on a Siemens D500 diffractometer (Cu Kα source) in flat plate $\theta/2\theta$ geometry. Data were recorded in the 15–100° 2θ-range with 0.05° step. The Rietveld method [10] was used as implemented in the package Fullprof [11] to analyze structural and microstructural properties. The particle size, size distribution and morphology of the powders prepared were examined by transmission electron microscope (TEM) using a CM30 SuperTwin transmission electron microscope operating at 300 kV. Specimens for electron microscopy were prepared by suspending the fine powder in an organic solvent on carbon grids. Specific surface areas of synthesized powders were measured by the Brunauer–Emmett–Teller (BET) isotherm technique with nitrogen adsorption using a Micromeritics ASAP 2000 surface area analyzer.

1.1.3. Screen-printing slurry and characterization of the 8YSZ dense layer

Electrolyte slurries consisting of 8YSZ synthesized or commercial (MEL-Chemicals) powder, terpineol (phosphate ester as a dispersant), ethylcellulose and dibutyl phthalate (DBT) were prepared and mixed in a planetary ball mill (Fristch Pulverissette 7) for 3 days. The slurry was screen printed (DEKJ 1202 RS) onto an alumina commercial substrate and subsequently fired at 1300 °C in air for 10 h. The temperature was increased at a rate of 5 °C/h up to the firing temperature, with an intermediate pause for 5 h at 1100 °C to improve densification [12]. The resulting layer characteristics were observed by scanning electron microscopy (SEM).

2. Results

2.1. Fluorite electrolyte materials: 8YSZ and CGO

Using the polyacrylamide-assisted method, after 5 h at 800 °C in air, single phase powders of 8YSZ and CGO were synthesized as shown in the XRD spectra (Fig. 1). We also shown in Fig. 1 the calculated XRD patterns as obtained from Rietveld refinements. All peaks can be assigned to the desired final compounds indexed on the basis of a cubic fluorite cell (space group:$Fm\bar{3}m$), with measured cell parameters as reported in Table 1. Crystal size evaluation by means of the Rietveld refinements and TEM images (Fig. 2) are in good agreement (Table 1). As an illustration of the

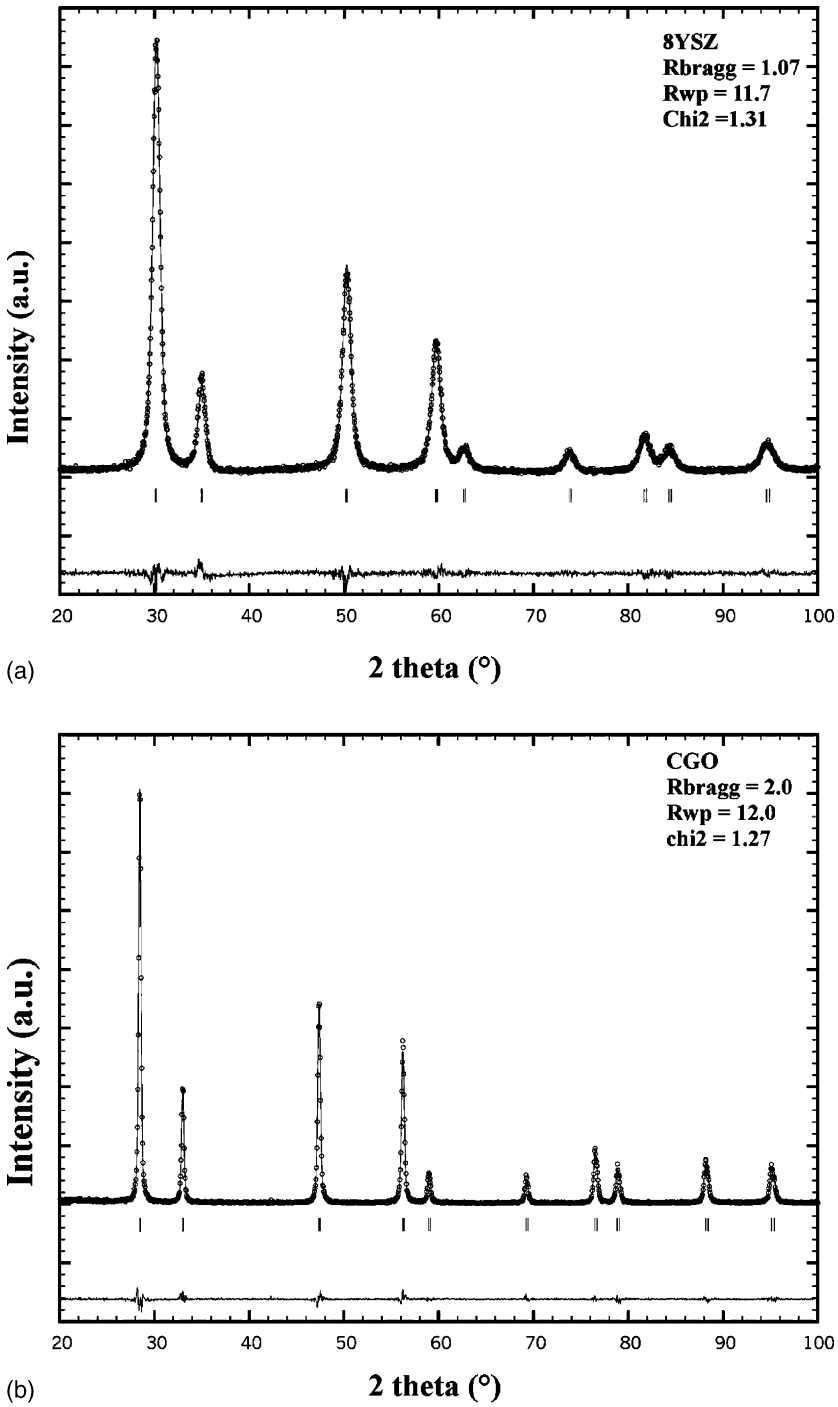

Fig. 1. Experimental (open circles), calculated and difference (solid lines) XRD patterns of (a) 8YSZ and (b) CGO samples. The vertical bars show the Bragg angle positions corresponding to a fluorite structure (SG: $Fm\bar{3}m$) with cell parameters as indicated in Table 1. Also are indicated the reliability factors R_{Bragg}, R_{wp} and χ^2 of Rietveld refinements.

Table 1
Microstructural properties of 8YSZ and CGO powders as determined from TEM, XRD Rietveld refinements and BET characterization

Sample	Grain size from XRD (±1 nm)	Grain size from TEM (±3 nm)	Specific surface (m^2/g)	Cubic cell parameter (Å)
8YSZ	9	12	13.56	5.1385(5)
CGO	35	39	5.36	5.4246(3)

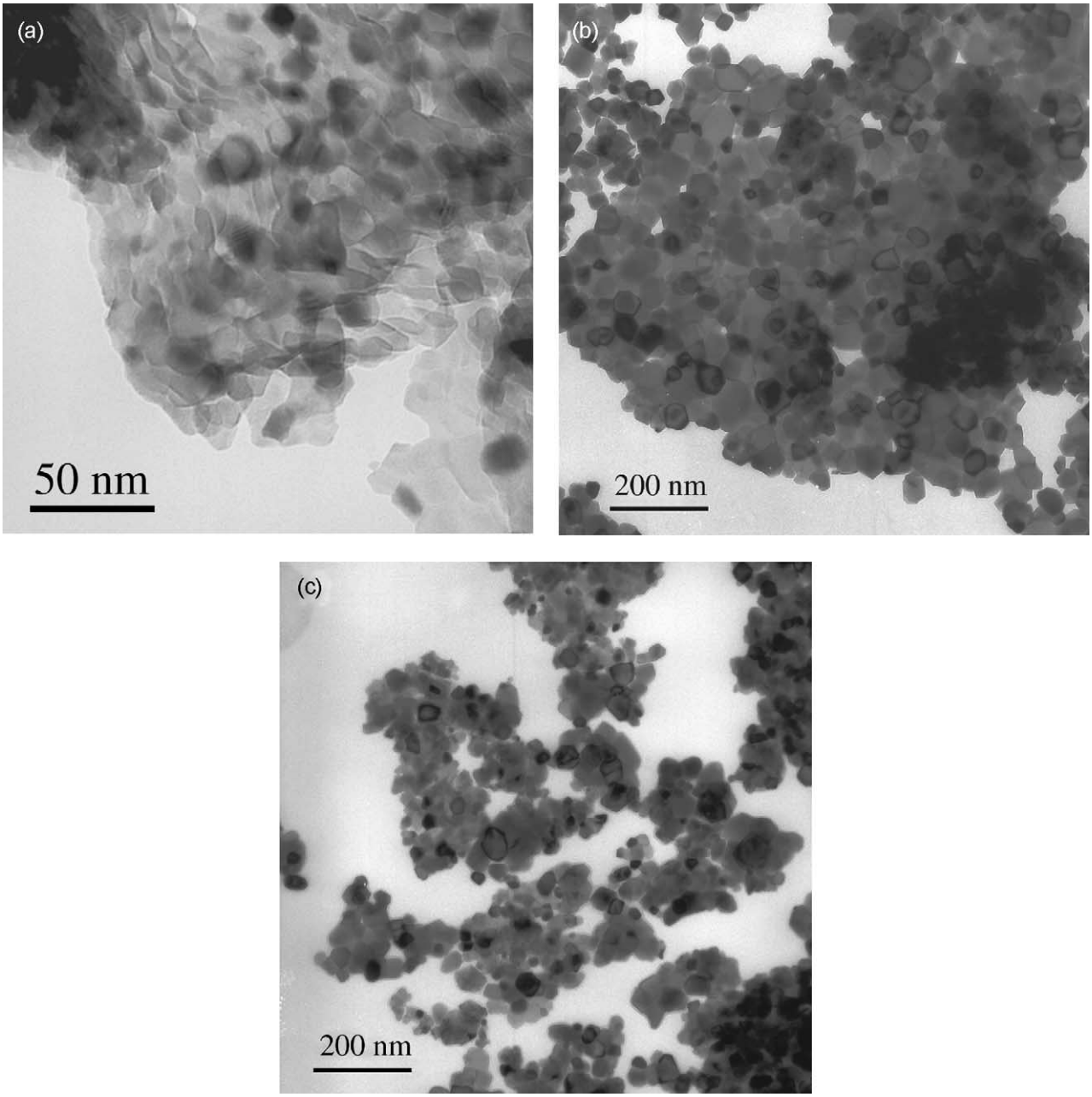

Fig. 2. TEM images of (a) 8YSZ sample, CGO sample (b) before and (c) after a short grinding (10 min in a planetary ball milling).

homogeneity of grain size, we present in Fig. 3, the grain size distribution measured on several hundreds of particles of the CGO sample. Both XRD and TEM techniques evidence a significantly smaller grain size of the 8YSZ sample compared to that of the CGO sample, despite the same calcination temperature. This difference is also reflected by the BET measurements which show a much smaller specific area (Table 1) for the cerium based fluorite sample. Similar results comparing zirconium and cerium-based fluorite oxides have been reported previously [13] and might be due to the better sinterability of cerium-based compounds. Actually, Li et al. [14] reported that 99% density cerium oxide ceramics could be obtained at a temperature as low as 1160 °C, while zirconia based ceramics are usually fully densified at temperatures of at least 1300–1400 °C [12].

Representative SEM photographs (Fig. 4a) show powder morphology consisting of aggregates with a flake-like aspect. In order to check the strength of the agglomerates, the CGO was ball-milled during 10 min. After this treatment, the general aspect of the powder evolves, changing from a foam-like powder to a less volume-occupying and more fluidic powder. This is due to the disagglomeration of the fine particles forming the plaques as evidenced by TEM images (Fig. 2b and c) and it confirms that nanometric grains are weakly linked as previously suggested [7].

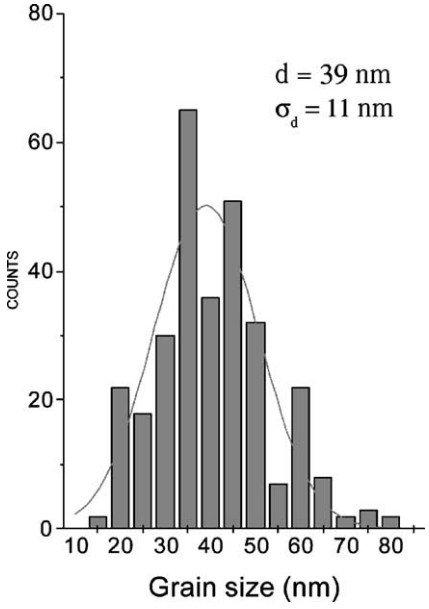

Fig. 3. Distribution of grain size measured by TEM for CGO sample.

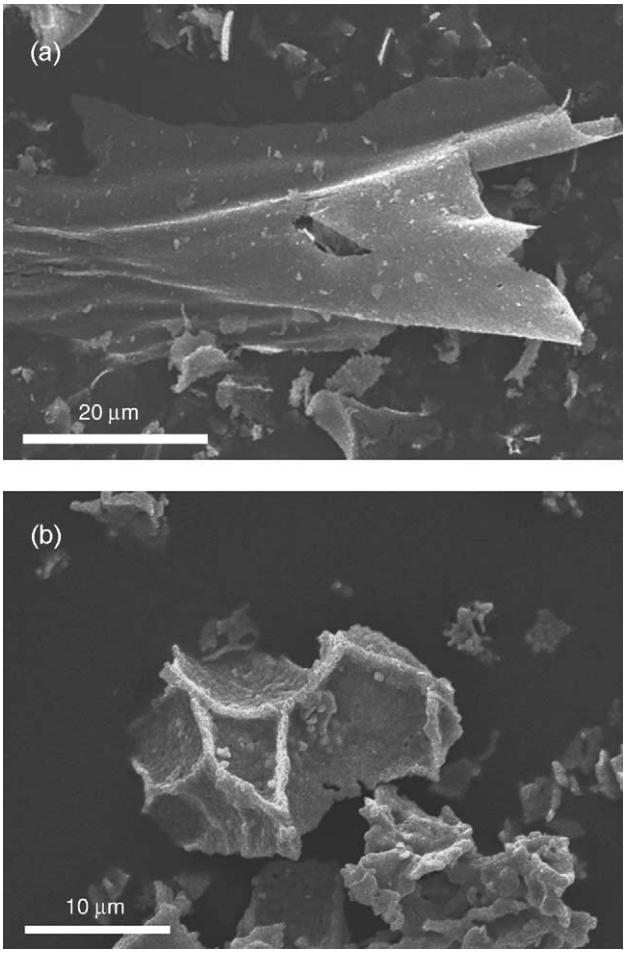

Fig. 4. SEM images of (a) CGO sample prepared from acrylamide and (b) $La_2Mo_2O_9$ sample prepared from methacrylamide.

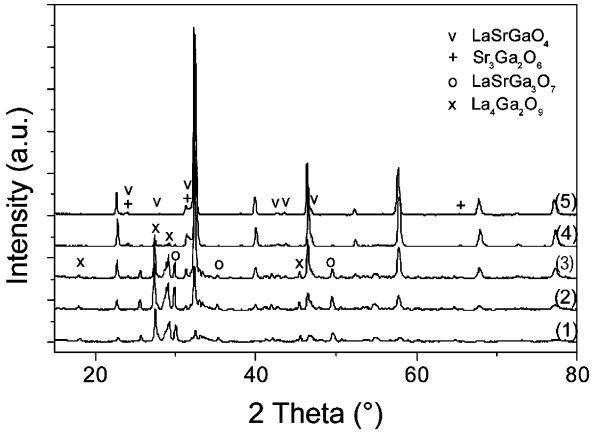

Fig. 5. XRD patterns of LSGM sample annealed at (1) 800 °C, (2) 900 °C, (3) 1000 °C, (4) 1100 °C, (5) 1300 °C during 5 h under air (the reflections not labeled correspond to the perovskite LSGM phase).

2.2. Perovskite electrolyte: LSGM

The phase evolution of the precursor with calcination temperature is shown in Fig. 5 by means of XRD measurements at 800, 900, 1000, 1100 and 1300 °C. The intermediate products up to 1100 °C are multiphase with the presence of $La_4Ga_2O_9$, $LaSrGa_3O_7$, $LaSrGaO_4$ and $Sr_3Ga_2O_6$. After a thermal treatment at 1300 °C during 5 h, the main phase is the $LaGaO_3$-derived perovskite phase, with small amounts of $LaSrGaO_4$ and $Sr_3Ga_2O_6$. The $Sr_3Ga_2O_6$ phase found in this work is neither mentioned in previous works involving sol–gel [15] or the Pechini, combustion and mixed oxide route [16] but it does appear when using the ultrasonic spray pyrolysis method [17]. The perovskite phase can be indexed in a cubic unit cell [18,19] with calculated cell parameter $a = 3.9078(5)$ Å. In fact, the real structure is probably orthorhombic with space group *Imma*, as revealed by a recent neutron study [20].

Synthesis of a pure single phase of LSGM is found to be rather difficult. Previous works conclude that, independently of preparation routes, calcination up to 1500 °C [16] is needed to reach a pure perovskite cubic single phase, because $LaSrGa_3O_7$ and $LaSrGaO_4$ are in thermodynamic equilibrium with LSGM at 1400 °C in air. Besides, it appears that small deviations from the ideal composition would result in the appearance of parasitic phases, due to a narrow composition range for the stability of the perovskite phase [19].

2.3. LAMOX family: $La_2Mo_2O_9$

Well crystallized $La_2Mo_2O_9$ was synthesized using methacrylamide as a less toxic substitute for acrylamide. The great majority of XRD reflections (Fig. 6) can be indexed in a cubic unit cell with a calculated cell parameter $a = 7.1545(5)$ Å. Nevertheless, some small intensity reflections are also observed at 29.5, 33.7, 38.8 and 40.6°. The presence of such diffraction peaks indicate that the real

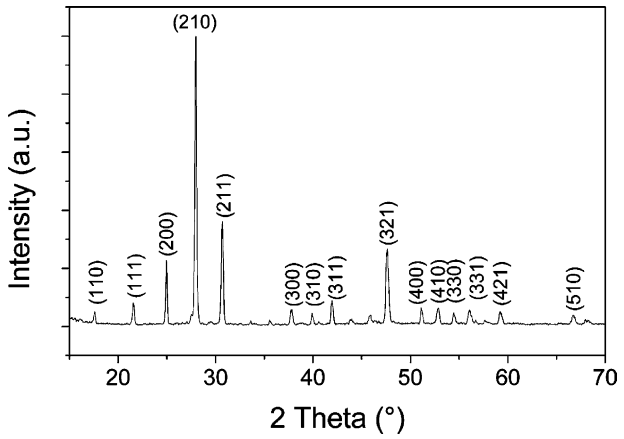

Fig. 6. XRD pattern of $La_2Mo_2O_9$ sample—indexation in a cubic unit cell ($a = 7.1545$ Å).

symmetry of such phase is probably lower, as previously mentioned by Goutenoire et al. [21]. SEM characterization (Fig. 4b) shows that the powder prepared from methacrylamide has a similar sponge-like morphology to those prepared from acrylamide, but with thicker sheets and more compacted aggregates. At a higher scale (not presented), we observed agglomerates with sintered particles of size around 500–1000 nm, which may indicate a low sintering temperature for such material. In fact, a previous work [22] shows that a temperature of 600 °C is sufficient to well crystallize $La_2Mo_2O_9$ using the sol–gel method.

2.4. Perovskite electrode materials: LSC and LSF

Electrode nanocrystalline materials can be produced by acrylamide polymerisation also. A particular case reported here concerns the synthesis of LSC and LSF perovskite compounds. In Fig. 7, we present TEM images where both LSC and LSF compounds prepared from acrylamide are shown, and also the LSC compound prepared from methacrylamide.

The calcination of LSC at a temperature as low as 800 °C for 5 h. produced material in which no unreacted single or binary metal oxides were detected. XRD analysis revealed that the main peaks can be indexed in a rhomboedral unit cell with cell parameters $a = 5.4488(4)$ Å and $c = 13.4764(9)$ Å. Nevertheless, several small reflections were observed, which can be associated with the formation of an orthorhombic vacancy-ordered phase as reported in [23]. Let us point out that, in that work, such a phase had been synthesized at low temperature and was shown to be the structural form with the highest conductivity. As shown in Fig. 7b and c, a comparison between acrylamide and methacrylamide-prepared samples seems to indicate a higher grain size for the latter. In fact, XRD revealed roughly the same coherent grain size ($d_{XRD} =$ 30(2) nm) for both phases. The error may come from a significant statistical error in the case of the TEM measurements.

Many problems with Fe(III) have been observed because it was an inhibitor to the polymerisation reaction. Several polymerisation attempts have been necessary to obtain the polyacrylamide gel. Weak gelification was finally achieved by adjusting pH at 6, the optimum value for Fe–EDTA complex formation, and reducing the cation concentration in solution. XRD analysis indicated that this compound should be indexed in an orthorhombic cell (SG: *Pnma*). Rietveld refinement permitted us to calculate lattice parameters—$a = 5.5429(3)$ Å, $b = 5.5398(3)$ Å, $c = 7.8432(9)$ Å—and the crystal size $d = 35(4)$ nm, which is significantly smaller than the one calculated ($d_{TEM} = 55$ (10) nm) on the basis of TEM pictures (Fig. 7a). Similarly to the LSC series, this difference may come from the small number of particles, $n = 20$, measured by TEM. Only the counting of a high number of grains may give a good indication of grain size, as in the case of fluorite compounds in which several hundreds of grains have been taken into account.

2.5. Screen printed dense thin film

SEM images presented in Fig. 8a and b show a full-density layer of 4 μm thickness for the film deposited from 8YSZ commercial powder by screen-printing. Starting from as-synthesized powders, a high level of densification is also achieved but some inhomogeneities can be observed (Fig. 8c). These screen-printing first results for dense electrolyte thin films of synthesized powder are very promising. Further works are in progress to achieve full density from synthesized powders due to their better a priori characteristics for sintering and consolidation. The benefits of finer powders have been clearly demonstrated in previous works concerning, for example, zirconia densification [12]. The main problem appears to be a greater tendency of nanoparticles to interact giving rise to the formation of agglomerates. Thus, special attention, in particular during the grinding step, must be paid to jump from partial to full-density layers.

3. Discussion

Many binary, ternary and quaternary oxide compounds have been prepared with success by acrylamide polymerisation. Independently of composition, all the as-prepared powders present a foam morphology with micron-scale sheet-like agglomerates made of many nanometric crystallites. Powders prepared by means of the similar nitrate/citrate gel-combustion method [24,25] also present the same morphology. In both cases, starting from nitrate salts of metallic cations, combustion is produced in which nitrate ions act as oxidizers for the combustion of an organic fuel. The excess of fuel does not participate in the combustion reaction but at higher temperatures it is burned generating a large amount of gas. Evolution of the gases produced promotes the disintegration of the native aggregates/precipitates giving final voluminous and fragile aggregates. As we have demonstrated, soft ball milling is sufficient to break the links between the spherical particles inside the agglomerates.

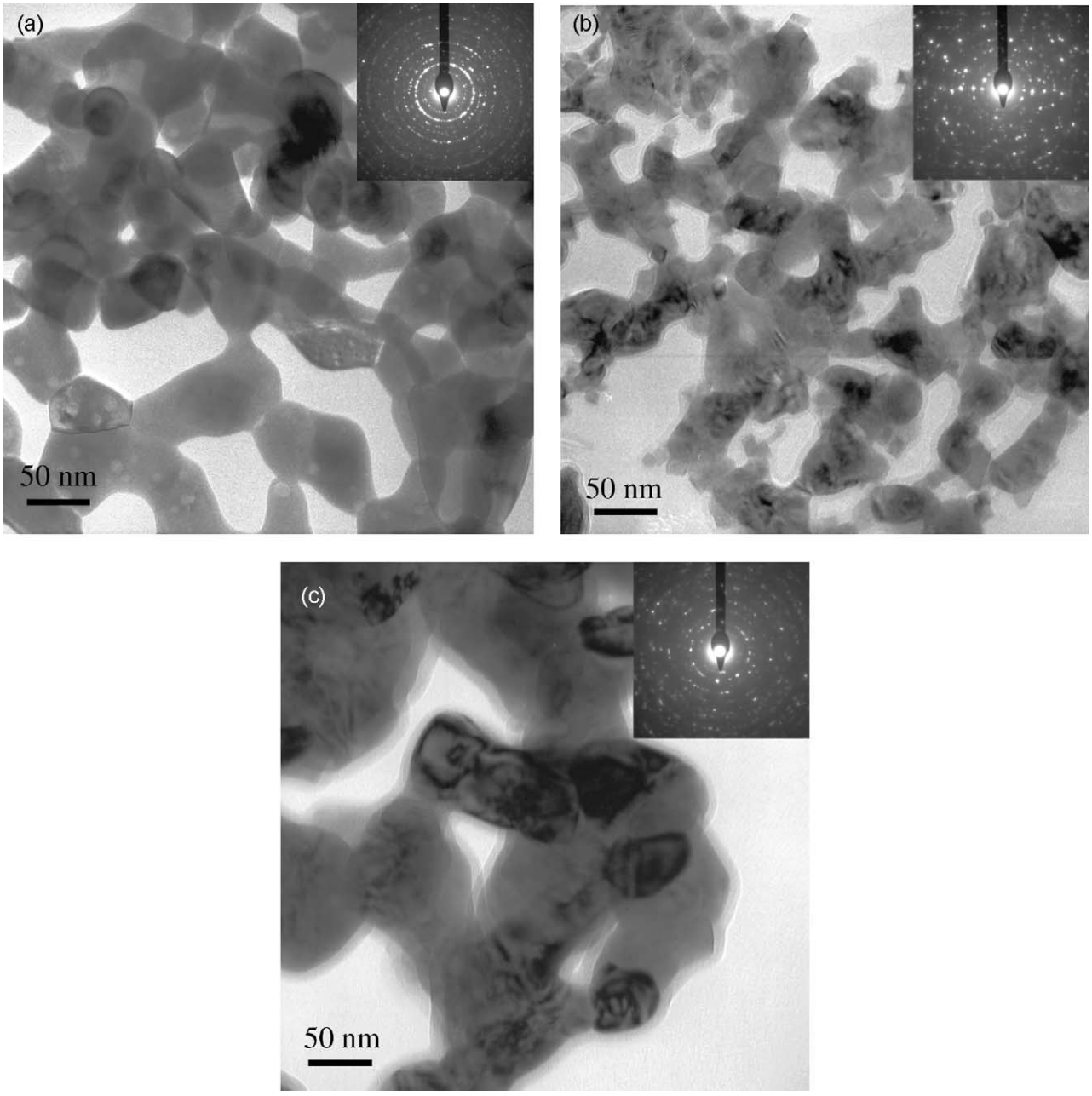

Fig. 7. TEM images of cathode perovskite powder samples: (a) LSF, (b) LSC from acrylamide and (c) from methacrylamide.

The high toxicity level of acrylamide forced us to search for an alternative monomer for gel constitution. A comparative study, from the authors, of methacrylamide and acrylamide synthesized powders (8YSZ) shows that similar properties were observed for powders prepared from the same amount of cation/monomers in solution. In this work, lanthanum molybdate and lanthanum strontium cobaltite were prepared by means of methacrylamide, obtaining excellent results from the point of view of crystallinity and purity of phases. Concerning microstructural properties, slight differences of agglomerate consistence were observed. Previous studies [7] conclude that the powder grain size obtained with acrylamide is independent of gel morphology, but could be strongly dependent on the combustion process [26]. This conclusion might be extrapolated to methacrylamide gels. Concerning morphology, SEM images suggest stronger nanoparticle agglomeration (thicker sheets) in methacrylamide, which could be due to more dilute gels obtained by means of methacrylamide or to different combustion kinetics.

A weak point of the polyacrylamide gel-assisted method resides in the retardation or inhibition of the polymerisation reaction by acrylamide–cation complexation specially for transition elements. Actually, the complexation of transition metal elements by acrylamide and the polymerisation of such complexes is still a matter of research. For instance,

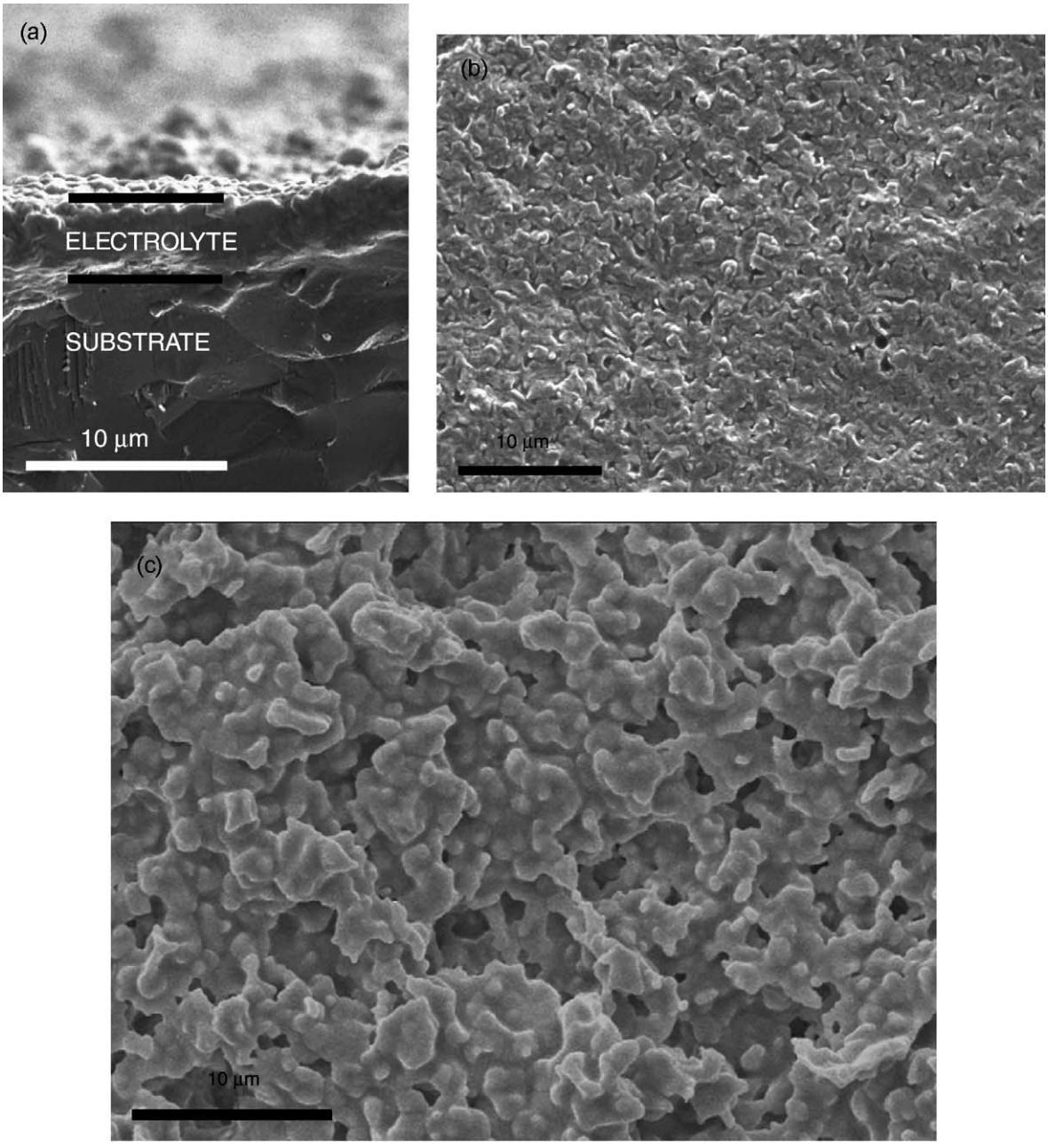

Fig. 8. SEM images of dense films deposited by screen-printing from (a and b) MEL commercial powders and (c) acrylamide-prepared powder.

metal cations Cr(III)–, Mn(II)–, Fe(III)–, Co(II)–, Ni(II)–, Cu(II)–, Zn(II)–acrylamide complexes in nitrate aqueous solution were synthesized and characterized, where it was shown that four acrylamide ligands can be bonded to each metal ion [27]. Such Mn–, Co–, Ni–, Zn–acrylamide complexes could be further polymerized upon heating [28,29]. On the other hand, in the case of Fe or Co cations, we were not able to obtain polyacrylamide gels without previous chelation (see below). Possibly, the complexation of cations by acrylamide significantly decreases the rate of the polymerisation reaction. Besides, the complexation of metal cations by bis-acrylamide should also be considered, as this may also diminish reticular polymerisation and impede the formation of the 3D tangled network. One could argue that, since the acrylamide and bis-acrylamide involved in complexation may not polymerize, the use of a higher content of monomers in solution or a lower cation concentration would overcome such a limitation. In fact, such solutions were also explored and led effectively to good results, with the limitation of lower powder production yield in the latter case and the possibility of polymer phase separation in the former when the concentration of monomers is too high. Alternatively, in order to avoid metal-complexation by acrylamide, it has been proposed to chelate the cation in solution by EDTA, before acrylamide and bis-acrylamide addition [7]. Indeed, EDTA is known as a good chelating agent for

transition metal cations, and has been widely used in chelation titration methods. The use of EDTA has allowed us to overcome the parasitic metal-complexation by acrylamide for many problematic cations [7]. While with Co cations the acrylamide polymerisation after EDTA addition occurred without problems, in the case of Fe cations, the final gel obtained seems to be significantly more fragile than in the case of Co, in spite of special care over pH conditions to optimize EDTA complexation. Taking into account the high affinity of iron cations for acrylamide, it is probable that the complexation reaction has been at least partially displaced from EDTA to acrylamide complexes. Let us mention that, apart from the iron-containing composition, for the other materials, we obtained a highly homogeneous gel with the use of the EDTA complexing agent. Also, it is worthwhile noting that in the case of 8YSZ, gelification can also be performed without the use of EDTA. Further studies are necessary to establish whether or not the use of EDTA is absolutely necessary and if acrylamide or bis-acrylamide can displace EDTA complexation.

4. Conclusion

Polyacrylamide gel-assisted synthesis as a wet chemistry rout permits us to synthesize ultrafine powders of a wide variety of ceramic materials with applicability in SOFC. In all cases, the powders synthesized at low temperatures (800 °C) are composed of micron-scale thin sheets formed of many nanocrystallites. Such flake-like agglomerates can be easily broken by a short ball milling. This is one of the most important points with a view to SOFC applications. Indeed, in relation to dense electrolytes, the size, size distribution, shape and state of agglomeration have important consequences for the sintering step and the final degree of densification. With a particle size of less than 50 nm and a narrow grain size distribution the achievement of high densities is a reasonable goal, as pointed out by our first results on screen-printing of dense films from these powders. Besides, in relation to electrodes and catalysis reactions, high specific surface area which can be easily achieved here is desired in order to maximize surface in contact with the fuel (anode) or air (cathode). The present wet chemistry method is time-saving when compared to other routes, and the versatility and robustness of this synthesis route and the interesting applicability to SOFC materials has been clearly demonstrated. Finally, we showed that we were able to synthesize the base–$La_2Mo_2O_9$ material, which opens up the possibility for the synthesis and study of new fast-oxide conductors in the LAMOX family.

Acknowledgements

This work has been supported by the Ministerio de Ciencia y Tecnologia of Spain (CICYT MAT-2000-0206-p403).

References

[1] J.C. Boivin, G. Mairesse Chem. Mater. 10 (1998) 2870.
[2] S.J. Skinner, Int. J. Inorg. Mater. 3 (2001) 113.
[3] P. Lacorre, F. Goutenoire, O. Bohnke, R. Retoux, Y. Lagilant, Nature 404 (2000) 856.
[4] R.H.E. van Doorn, A.J. Burggraff, Solid State Ionics 128 (2000) 65.
[5] M.P. Pechini. US Patent No. 3330697 (1967).
[6] G. Dezanneau, A. Sin, H. Roussel, H. Vincent, M. Audier, Solid State Commun. 121 (2002) 133–137.
[7] A. Sin, P. Odier, Adv. Mater. 12 (2000) 649–652.
[8] A. Douy, Int. J. Inorg. Mater. 1 (2001) 699.
[9] C. Xia, F. Chen, M. Liu, Electr. Solid State Lett. 4 (2001) A52.
[10] H.M. Rietveld, Powder Diffr. 2 (1969) 65.
[11] J. Rodriguez-Carvajal, Powder diffraction, in: Proceedings of the Abstracts of the Satellite Meeting of the XV Congress of the International Union of Crystallography, Toulouse, 16–19 July 1990, p. 127.
[12] O.C. Standard, C.C. Sorell, Key Eng. Mater. 153–154 (1998) 251.
[13] I. Kosacki, T. Suzuki, V. Petrovsky, H.U. Anderson, Solid State Ionics 136–137 (2000) 1225.
[14] J.G. Li, T. Ikegami, J.H. Lee, T. Mori, Acta Mater. 49 (2001) 419.
[15] K. Huang, B. Goodenough, J. Solid State Chem. 136 (1998) 274.
[16] P. Majewski, M. Rozumek, C.A. Tas, F. Aldinger, J. Electrochem. 8 (2002) 65.
[17] E. Djurado, M. Labeau, J. Eur. Ceram. Soc. 18 (1998) 1397.
[18] K. Huang, M. Feng, J.B. Goodenough, J. Am. Ceram. Soc. 79 (1996) 100.
[19] K. Huang, J.B. Goodenough, J. Alloys Comp. 303–304 (2000) 454.
[20] M. Lerch, H. Boysen, T. Hansen, J. Phys. Chem. Solids 62 (2001) 445–455.
[21] F. Goutenoire, O. Isnard, R. Retoux, P. Lacorre, Chem. Mater. 12 (2000) 2575.
[22] W. Kuang, Y. Fan, K. Yao, Y. Chen, J. Solid State Chem. 140 (1998) 354.
[23] J. Kirchemova, D.B. Hibbert, Mater. Res. Bull. 25 (1990) 585.
[24] L. Fraigi, D.G. Lamas, N.E. Walsöe de Reca, Nanostruct. Mater. 11 (1999) 311.
[25] M. Marinsek, K. Zupan, J. Maèek, J. Power sources 106 (2002) 178.
[26] A. Sin, J.J. Picciolo, R.H. Lee, F. Gutierrez-Mora, K.C. Goretta, J. Mater. Sci. Lett. 20 (2001) 1639–1641.
[27] V.S. Svost'yanov, V.I. Ponomarev, A.D. Pomogailo, B.S. Selenova, I.N. Ivleva, A.G. Starikov, L.O Atovmyan, Izv. Akad. Nauk SSSR, Ser. Khim. 762 (1990) [Bull. Acad. Sci. USSR, Div. Chem. Sci. 39 (1990) 674].
[28] V.S. Svost'yanov, A.D. Pomogailo, B.S. Selenova, D.A. Kritskaya, A.N. Ponomarev, Izv. Akad. Nauk SSSR, Ser. Khim. 768 (1990) [Bull. Acad. Sci. USSR, Div. Chem. Sci. 39 (1990) 680].
[29] V.S. Svost'yanov, G.P. Belov, D.A. Kritskaya, A.D. Pomogailo, A.N. Ponomarev, Izv. Akad. Nauk SSSR, Ser. Khim. 1015 (1990) [Bull. Acad. Sci. USSR, Div. Chem. Sci. 39 (1990) 6905].